Published in final edited form as:
Structure. 2010 October 13; 18(10): 1270–1279. doi:10.1016/j.str.2010.07.009.

Crystal structure of group II chaperonin in the open state

Yanwu Huo[1,7], **Zhongjun Hu**[1,6,7], **Kai Zhang**[1,7], **Li Wang**[2], **Yujia Zhai**[1], **Qiangjun Zhou**[1], **Gabe Lander**[3], **Jiang Zhu**[4], **Yongzhi He**[2], **Xiaoyun Pang**[1], **Wei Xu**[1], **Mark Bartlam**[5], **Zhiyang Dong**[2,*], and **Fei Sun**[1,*]

[1]National Laboratory of Biomacromolecules, Institute of Biophysics (IBP), Chinese Academy of Sciences, Beijing 100101, China

[2]The State Key Laboratory of Microbial Resources, Institute of Microbiology, Chinese Academy of Sciences, Beijing 100101, China

[3]The Scripps Research Institute, 10550 North Torrey Pines Rd, La Jolla, CA 92037, U.S.A.

[4]Vaccine Research Center, National Institute of Allergy and Infectious Diseases, National Institutes of Health, 40 Convent Dr., Bethesda, MD 20892-3027

[5]College of Life Sciences, Nankai University, Tianjin, China

[6]Department of Physics, Logistics Engineering University, Chongqing 401311, China

SUMMARY

Thermosomes are group II chaperonins responsible for protein refolding in an ATP-dependent manner. Little is known regarding the conformational changes of thermosomes during their functional cycle due to lack of high-resolution structure in open state. Here we report the first complete crystal structure of thermosome (rATcpnβ) in open state from *Acidianus tengchongensis*. There is a ~30° rotation of the apical and lid domains compared to the previous closed structure. Besides, the structure reveals a conspicuous hydrophobic patch in the lid domain and residues locating in this patch are conserved across species. Both the closed and open forms of rATcpnβ were also reconstructed by electron microscopy (EM). Structural fitting revealed the detailed conformational change from open to closed state. Structural comparison as well as protease K digestion indicated only ATP binding without hydrolysis does not induce chamber closure of thermosome.

[*]Correspondence should be addressed to, Fei Sun, Ph.D, Laboratory of Biological Electron Microscopy and Structural Biology, Institute of Biophysics, Chinese Academy of Sciences, 15 Datun Road, Chaoyang District, Beijing 100101, China, Tel/Fax: + 86-(10)-64888582, feisun@ibp.ac.cn Or Zhiyang Dong, Ph.D, Tel: + 86-(10)-64807337, Fax: + 86-(10)-64807337, dongzy@sun.im.ac.cn.
[7]These authors gave equal contributions to this work.

ACCESSION NUMBERS

The rATcpnβ negative staining electron microscopy density map and the rATcpnβ_apo and rATcpnβ_ATP cryo-electron microscopy density maps were deposited in Electron Microscopy Data Bank (EMDB) with the access number EMD-5154, EMD-5159 and EMD-5157, respectively. The rATcpnβ_ADP crystal structure coordinates were deposited in the Protein Data Bank (PDB) with accession number 3KO1.

Keywords

Group II chaperonin; Thermosome; Open state; Conformational change

INTRODUCTION

Chaperonins are a class of molecular chaperones (Hemmingsen et al., 1988), oligomeric complexes that act as protein folding cages and facilitate proper protein folding through ATP consumption. Chaperonins have been classified into two subfamilies (group I and group II) based on their structure and sequence (Kim et al., 1994). Group I chaperonins exist in bacteria, mitochondria and chloroplasts, as exemplified by the well-studied *E. coli* chaperonin GroEL (Bukau and Horwich, 1998; Ranson et al., 2006). Group II chaperonins are found in archaea (Phipps et al., 1991) or eukaryotic cytosol (Frydman et al., 1992; Gao et al., 1992). Archaeal group II chaperonins are also referred as thermosomes due to their extreme thermal stability (Bigotti and Clarke, 2008). In eukaryotes, the cytosolic group II chaperonin containing TCP-1 (CCT) is reported to facilitate the correct folding of cellular cytoskeletal elements such as actin and tubulin (Gao et al., 1992; Yaffe et al., 1992).

A common feature shared by group I and II chaperonins is a characteristic double ring structure, in which each subunit contains three domains: an equatorial domain that contains an ATP-binding site and is involved in inter-ring contacts, an apical domain for substrate binding and an intermediate domain that connects the equatorial and apical domains via flexible hinges (Ditzel et al., 1998; Xu et al., 1997). One of the major differences between these two groups is that group I requires the cofactor GroES (Tilly et al., 1981) to form a single ring and enclose the cage, whereas group II has a covalently attached lid domain that extends from the apical domain to cover the cage (Ditzel et al., 1998). Another difference is that whereas a group I chaperonin always consists of two homo-heptameric rings (Xu et al., 1997), each ring of a group II chaperonin consists of eight or nine hetero- or homo-subunits (Ditzel et al., 1998; Frydman et al., 1992; Schoehn et al., 2000; Shomura et al., 2004; Xu et al., 1997).

Before this work, two available crystal structures of thermosomes from both *Thermoplasma acidophilum* (Ditzel et al., 1998) and *Thermococcus sp.* strain KS-1 (Shomura et al., 2004) were shown to adopt a tightly closed conformation, exhibiting apical domains and inter-ring contacts that differ from group I chaperonins. However, various conformations of group II chaperonins were described by cryoEM reconstruction, including closed forms, open forms and asymmetric bullet-shaped forms, indicating the existence of domain movement during their functional cycles (Clare et al., 2008; Schoehn et al., 2000). In the absence of nucleotides, both thermosomes and CCT were found to have an open form (Llorca et al., 1999; Nitsch et al., 1998). Furthermore, the open and closed states of CCT have recently been comparatively modeled based on middle resolution cryoEM maps, suggesting that the lid closure was achieved by ~25° rotation of the intermediate domain and additional 50° rotation of the apical domain towards the equatorial domain(Booth et al., 2008). However, comparison between 8Å cryoEM structure of thermosome Mm-cpn in open state and its 4.3Å cryoEM structure in closed state suggested the chamber closure was completed by the inward movement of entire subunit (Zhang et al., 2010). As a result, the detailed conformational changes during transition from open to close is still not well-characterized due to the lack of a high-resolution structure for group II chaperonin in open state. Furthermore, the substrate binding determinants are unclear for group II chaperonins. Besides, there are two models describing the transition from open to closed state. One model suggests that the binding of ATP triggers chamber closure (Iizuka et al., 2003), while the other model suggests that it is the ATP hydrolysis to induce the closed conformation (Bigotti

and Clarke, 2008). Those questions are importantly related to understand the molecular function of group II chaperonin and need to be carefully investigated.

The archaea *Acidianus tengchongensis* strain S5 grows in the Tengchong acidothermal springs in Southwestern China with an optimal temperature of 70 °C and pH of 2.5. Two genes of this archaea (cpnα and cpnβ) were found to encode two types of chaperonin subunits (ATcpnα and ATcpnβ) that can assemble into thermosomes either homogenously or heterogeneously (Wang et al., 2010). Preliminary studies have shown that recombinant ATcpnα (rATcpnα) assembles into an 8-fold double ring structure, recombinant ATcpnβ (rATcpnβ) into a 9-fold structure and a combination of rATcpnα and rATcpnβ assembles into a 9-fold hetero-oligomer with 1:2 stoichiometry (Wang et al., 2010). Both of hetero-oligomer and homo-oligomer show trace ATP hydrolysis activity and limited refolding activity in vitro (Wang et al., 2010).

In this study, we focus on describing the 9-fold structures of rATcpnβ by X-ray crystallography and electron microscopy. We solved the first high-resolution (3.7Å) structure of complete group II chaperonin in its open state and found that its conformational changes from open to closed state are achieved by both ~30° intrinsic rotation of lid and apical domains and the inward movement of entire subunit. The conspicuous hydrophobic patch in the lid domain was found conserved across species and believed as a potential substrate-binding site. Structural analysis and protease K digestion assay suggested only ATP binding without hydrolysis could not trigger a closed structure for group II chaperonin.

RESULTS AND DISCUSSION

Crystal structure of rATcpnβ in the open state

The protein rATcpnβ was cloned, heterogeneously expressed in *E. coli* and purified by chromatography. Purified rATcpnβ was assembled into thermosomes *in vitro* under proper conditions (see **Experimental procedures**). The rATcpnβ thermosome complexes (if not indicated, rATcpnβ will be used to represent the rATcpnβ thermosome discussed below) were successfully crystallized into two different crystal forms (Form I and Form II). Both Form I and Form II share the same C2 space group, although Form I crystals have a larger unit cell than Form II (Table 1). Using the Matthews coefficient estimation, 27 rATcpnβ monomers (one and a half of rATcpnβ thermosomes) were calculated to occupy the asymmetrical unit of Form I, and 9 monomers (half of a rATcpnβ thermosome) of Form II. The crystal structures of Form I and Form II were determined by molecular replacement using a model built from the cryoEM map of rATcpnβ and were finally refined to 3.8Å (Rwork 36.5% and Rfree 37.1%) for Form I and to 3.7Å (Rwork 27.7% and Rfree 28.3%) for Form II. The statistics of data collection and structural refinements are summarized in Table 1. Although the structure determined in Form I is similar to that of Form II, the better diffraction data quality of Form II resulted in a more precise map (Figure S1). For this reason, only the Form II crystal structure was used for further analysis.

Of the 553 residues present in each rATcpnβ subunit, residues 1–27 and 533–553 were not assigned due to the lack of electron density. The rATcpnβ subunit itself shares a common fold with other group II chaperonins, consisting of an equatorial (residues 28–149 and 412–532), intermediate (residues 150–224 and 377–411), apical (residues 225–252 and 283–376) and lid domain (residues 253–282) (Figure 1A and B). The equatorial domain contains a seven-helix bundle (H1-H4-H12-H13 and H3-H5-H16) flanked by three helices (H2, H14 and H15) and five β-strands (S1, S2, S15, S16 and S17). The β-strands S1 and S2 form a β-sheet by interacting with the strand S17 from the adjacent subunit. The intermediate domain is mainly made up of a three-helix bundle (H6, H7 and H11) next to a two stranded β-sheet (S4 and S14). The apical domain contains two β-sheets (S5-S6-S12-S13 and S7-S8-S9-S10-

S11) surrounded by two α-helices (H9 and H10) above and below. The protruding lid is mainly comprised of α-helix H8 and a flexible loop between H8 and S7. The nucleotide binding site is located directly above the equatorial domain, as evidenced by a clear density in the omit 2FoFc map (Figure 1C).

In contrast to the thermosome crystal structures from *Thermoplasma acidophilum* (TAcpn) (Ditzel et al., 1998) and *Thermococcus sp.* strain KS-1(TKcpn) (Shomura et al., 2004), both of which adopt a closed form with 8-fold symmetry which might be caused by high concentration of ammonium sulfate in the crystallization buffer, the crystal structure of rATcpnβ exhibits an open conformation with 9-fold symmetry. Superposition of the rATcpnβ and TAcpnα/TAcpnβ/TKcpn subunits yields a large structural RMSD (root mean square deviation) of 1.4/1.7/2.4Å for the 460/468/470 Cα atoms, respectively (Figure 2A), despite a high sequence homology (75% sequence similarity and 54% identity, Figure S2). The individual domains (equatorial, intermediate, apical and lid) of rATcpnβ and TKcpn were further compared by superposition, yielding RMSD values of 1.0/0.8/0.9/1.3Å for the 217/93/115/25 Cα atoms, respectively. The high degree of structural similarity among the apical, intermediate and equatorial domains demonstrates that these domains are not flexible. The high RMSD value of the lid domain is due to its inherent structural plasticity (Ditzel et al., 1998; Klumpp et al., 1997). The different structural conformations between the rATcpnβ and TKcpn monomers are due to domain rotation and flexibility of the lid domain (Movie S1 and S2). There is a ~30° rotation of the apical and lid domain between rATcpnβ and TKcpn monomers (Figure 2A).

In Form II crystals, two asymmetric units make up the complete rATcpnβ thermosome, comprising two stacked, nine-subunit rings correlated by the crystallographic 2-fold axis. The rATcpnβ thermosome adopts an open state that differs from all previously reported closed structures (Ditzel et al., 1998; Shomura et al., 2004), exhibiting an overall cylindrical shape with a height of 185Å along the 9-fold axis and a diameter of 168Å along the 2-fold axis (Figure 1D and E). Each subunit has a surface area of 25600$Å^2$. The intra-ring contacts between adjacent subunits are localized mainly at the equatorial domains through interactions mediated by β-strands S1, S2 and S17, with a surface area of about 970$Å^2$ (Figure 1A and 1D). For inter-ring interaction, each subunit interacts with only one subunit of the opposite ring through its equatorial domain. This inter-ring contact interface is about 630$Å^2$, with electrostatic interactions mediated by eight pairs of salt bridges.

Around the inner surface of the chamber, there is a conspicuous hydrophobic patch located in the lid domain, which is composed of residue Ala262, Ile264, Ile266, Pro269, Met272, Phe275 and Leu276 (Figure 1F and G). Based on the sequence alignment of thermosome among representative species, it was found that those residues are highly conserved with two invariant residues Pro269 and Phe275 across species (Figure 1G), suggesting those residues might be the substrate binding determinants.

Electron microscopy study of rATcpnβ and structural fitting

We prepared the purified rATcpnβ sample in the presence and absence of ATP (referred to below as rATcpnβ_ATP or rATcpnβ_apo, respectively) for cryo-electron microscopy (cryoEM) studies. Two-dimensional image analysis, intensive 2D classification and averaging of more than 40,000 rATcpnβ_apo/rATcpnβ_ATP particle images revealed many classes with top views of 9-fold symmetry and a small portion (~10%) of 10-fold symmetry (Figure 3A and B) that was confirmed by blue native PAGE (Figure S3). Three-dimensional cryoEM structures of rATcpnβ_apo and rATcpnβ_ATP with imposed 9-fold symmetry were reconstructed with resolution 8.8Å and 8.4Å that were determined by RMEASURE respectively (Sousa and Grigorieff, 2007). Both cryoEM structures share similar cylindrical shape with a diameter of 173Å and a height of 180Å and exhibit an open conformation with

the bottom lid domain density missing (Figure 3C). Interestingly, the top lid domain density is much clearer in rATcpnβ_ATP than in rATcpnβ_apo, which suggests the flexibility of lid domain is reduced after ATP binds to thermosome. In accordance with the open crystal structure, the inter-ring and intra-ring contacts in cryoEM maps are only involved in the equatorial domains and the intermediate and apical domains are disconnected.

Docking the thermosome TKcpn subunit structure (PDB 1Q3R) en bloc into the cryoEM map of rATcpnβ_ATP doesn't yield good fit (Figure S4). The octadecamer model built by fitting eighteen TKcpn subunits into the cryoEM map shows severely loose intra-ring interactions, invalidating such a model (Figure S5). Docking the crystal structure of the rATcpnβ subunit into the same cryoEM density, all equatorial, intermediate and apical domains exhibit an excellent fit. By observation, most structural elements (α-helices, β-sheets and loops) fit the density tubes, layers and blobs precisely (Figure 3D). Most importantly, the helical protrusion of the lid domain fits well into lid density of the upper ring (Figure 3D), indicating that the crystal structure of rATcpnβ shares the same open state observed in the cryoEM map.

Although different conditions were tried many times, no rATcpnβ structure in closed conformation could be found by cryoEM study at all. However, the rATcpnβ thermosome examined by negative staining electron microscopy (nsEM) appears as a 9-fold closed structure (Figure 4). The relatively even orientation distribution enabled us to reconstruct the structure of rATcpnβ to 14Å resolution that was assessed by RMEASURE (Sousa and Grigorieff, 2007). The overall nsEM structure exhibits an oblong sphere shape with a diameter of 170Å and a height of 160Å (Figure 4C). Its particularly salient feature is that both rings adopt a closed conformation.

The crystal structure of rATcpnβ subunit could not fit into either the top or bottom ring of nsEM map very well (Figure S4). The octadecamer model built by fitting eighteen rATcpnβ subunits into the nsEM map shows severe structural collisions around the lid domain, indicating that it is an incorrect model (Figure S5). Whereas, docking the subunit from the crystal structure of closed-state TKcpn thermosome into the nsEM map provides a fairly good fitness (Figure 4D). Due to the good fitness and low resolution of nsEM map, the fitted model was not further optimized by flexible modeling tools. Those structural fitting indicate that the nsEM structure of rATcpnβ share the same closed conformation with the closed structure of TKcpn but not the open structure of rATcpnβ.

Implication based on structural comparison and analysis

It might be considered that whether the subunit conformational difference between the rATcpnβ open structure and the TKcpn closed structure is derived from their different symmetries. The conclusion is negative since that the 8-fold structure of rATcpnα was also successfully reconstructed by cryoEM and shows an open conformation (unpublished data), which could be fitted very well by the crystal structure of rATcpnβ but not by the TKcpn structure. As a result, sharing with very high sequence homology, such large conformational difference between rATcpnβ and TKcpn should have their biological significance.

All of above, it is clear that either cryoEM structures or crystal structure of rATcpnβ depict the similar open conformation, while the nsEM structure of rATcpnβ has a closed conformation. Supposing these two different conformations represent their biological state, it is necessary to compare them further and investigate the conformational change during transition from open to closed state. The rATcpnβ thermosome models in open and closed form were aligned after superimposing their 9-fold axes and equatorial planes, exhibiting large conformational changes (Figure 2B). Both a ~30° counterclockwise rotation of the apical and lid domains and an inward movement of the entire subunit were found to be

indispensible for transition from open to closed state (Movie S3, S4 and S5), which fixed the previous confused reports that lid closure of CCT needs domain rotation (Booth et al., 2008) but closing chamber of thermosome Mm-cpn requires the inward movement of entire subunit (Zhang et al., 2010). In addition, only the rotation of the lid and apical domains was observed for rATcpnβ and there is no rotation for intermediate domain with respect to equatorial domain, which is different to the medium-resolution cryoEM study of CCT (Booth et al., 2008). Upon the high-resolution structure of rATcpnβ in open state, the detailed conformational changes described in this work are much clearer and more accurate than before. Furthermore, such kind of conclusion was even strengthened when we compared the open cryoEM model of 8-fold rATcpnα with the crystal structure of closed TKcpn thermosome and found the exact same conformational changes (unpublished data).

What kinds of biological states do the open structures of rATcpnβ represent? The 2FoFc omit map in the crystal structure of rATcpnβ indicates it is a nucleotide-binding structure (Figure 1C). The nucleotide was further analyzed by high performance liquid chromatography experiments and recognized as ADP. Comparison between the cryoEM maps of rATcpnβ_apo and rATcpnβ_ATP showed clear additional density at the nucleotide-binding site in rATcpnβ_ATP (Figure 5A), which confirmed that the open structures of rATcpnβ_ATP and rATcpnβ_apo represent the ATP-binding state and nucleotide-free state respectively. As a result, it is clear that nucleotide binding would not trigger the nucleotide-free structure of rATcpnβ from open state to closed state, which was further proved by protease K digestion experiments. In the presence of different nucleotides (ATP or ADP), the rATcpnβ thermosome exhibits sensitivity to protease K digestion (Figure 5B), indicating it keeps the open conformation with or without nucleotide binding because it was reported that the closed thermosome was resistant to cleavage by protease (Iizuka et al., 2003). The fact that ATP binding does not induce a closed structure of rATcpnβ is different from Mm-cpn and CCT (Booth et al., 2008; Zhang et al., 2010). We further conclude that it is not due to the temperature because the protease K digestion experiment was carried at physiological temperature. Meanwhile we incubated rATcpnβ thermosome in its physiological temperature with the presence of ATP and AlF_3 before rapid freezing and did not find the closed structure by the subsequent cryoEM study. We speculate that it is the low ATP hydrolysis activity of rATcpnβ (Wang et al., 2010) to keep ATP bound to rATcpnβ without hydrolysis and enable us to observe the authentic open structure of rATcpnβ in ATP bound state. In contrast, when Mm-cpn thermosome or CCT was mixed with ATP and AlF_3, ATP will be hydrolyzed into ADP and the ATP hydrolysis transition state could be only captured. As a result, our structural study would further support the opinion that only ATP binding without hydrolysis could not drive the conformation from open to closed state for group II chaperonin.

Conclusions

Before this work, without a high-resolution structure of group II chaperonin in open state, researchers could only separate the closed crystal structure into equatorial, intermediate and apical domains and fit the individual domains into the open state cryoEM map to obtain a pseudo atomic model of group II chaperonin in open state (Booth et al., 2008; Clare et al., 2008). Here, we presented the first high-resolution (3.7Å) complete structure of group II chaperonin in open state which could be fit into open state cryoEM map perfectly so that the conformational changes from the open to closed state could be precisely described in details. In our study, it is found that the detailed conformational changes during transition from open to closed state could be achieved by ~30° intrinsic rotation of lid and apical domains and the inward movement of entire subunit. Either domain rotation or subunit movement alone could not complete the chamber closure of group II chaperonin. Furthermore, the conspicuous hydrophobic patch in the lid domain was found conserved across species and

might be a potential substrate-binding site that needs to be further investigated. Structural analysis and protease K digestion assay suggested only ATP binding without hydrolysis could not trigger a closed structure of group II chaperonin.

EXPERIMENTAL PROCEDURES

Molecular cloning of rATcpnβ

The molecular cloning of rATcpnβ was performed as recently reported(Wang et al., 2010). Briefly, genomic DNA of *Acidianus tengchongensis* strain S5 was prepared as described by Lauerer et al(Lauerer et al., 1986). The complete sequence of rATcpnβ gene was measured by inverse PCR(Ochman et al., 1988). The cDNA of rATcpnβ was amplified by PCR taken the genomic DNA as template and then sub-cloned into pET23b within NdeI and BamHI restriction sites.

Expression and purification of rATcpnβ

The rATcpnβ protein was overexpressed in the *E. coli* strain Rosetta-gami™ *B(DE3)pLysS* (Novagen) using the pET23b expression vector (Novagen). The recombinant bacteria were grown in Terrific Broth medium (TB) at 37°C. When the optical density (OD) of the culture at 600 nm reached 1.6~1.8, isopropyl β-D-1-thiogalactopyranoside (IPTG) was added to a final concentration of 0.4 mM. The culture was further incubated for 20 hr at 16°C. The harvested cells were broken in buffer A (20 mM Tris-HCl, pH 8.0, 5 mM EDTA-Na, 5 mM $MgCl_2$) by sonication. After centrifugation for 20 min at 10,000 g, the supernatant was incubated at 80°C for 30 min. After further centrifugation for 20 min at 10,000 g, the supernatant was applied to the Q-Sepharose fast flow column (GE Healthcare) that was pre-equilibrated by buffer A. After washing, the column was eluted using a linear NaCl gradient from 0 to 0.6 M in buffer A. The target rATcpnβ protein was eluted at 0.14 M NaCl, fractionated and dialyzed against buffer A overnight at 4°C. After dialysis, the protein was treated with 0.25 mM ATP and 1 M $(NH)_2$ SO_4 at 37°C for 5 hr to facilitate rATcpnβ assembly and then concentrated using an Amicon Ultra-15 filter (Millipore). The concentrated solution was applied to the Superdex 200 10/300 GL column (GE Healthcare), and the fully assembled rATcpnβ thermosomes were eluted using buffer A, separate from the monomers. The fractions were collected, concentrated to ~20 mg/ml and stored at −80°C. The purity of rATcpnβ was analyzed by SDS-PAGE and blue native PAGE.

Blue native PAGE

The concentration of the sample gel was 4% and the gradient separation gel concentration ranged from 5% to 13%. The loading amount of sample was about 100μg. Blue native PAGE (BN-PAGE) was performed at 4°C in a vertical apparatus with a deep blue cathode buffer B (50mM Tricine, 7.5mM imidazole, pH 7.0, 0.02% Coomassie blue G-250). At the beginning of the gel running, the electrophoresis voltage was maintained at 100V until the sample entered into the sample gel. Then the electrophoresis current was kept as a constant 15mA and the electrophoresis voltage was limited to below 500V. After about one-third of the total running distance, the cathode buffer B was replaced by cathode buffer B/10 for overnight electrophoresis(Wittig et al., 2006). After running BN-PAGE the gel was stained by Coomassie blue R250.

Electron microscopy, image processing and 3D reconstruction

For negative staining electron microscopy, 5 μl of 1 mg/ml rATcpnβ was applied to a glow-discharged carbon-coated grid that was stained with 5μl of 2% uranyl acetate. The negative stained rATcpnβ was imaged on a transmission electron microscope Tecnai T20 (FEI, Netherlands) with a LaB_6 electron source, operated at 200 kV. The electron micrographs

were recorded on a 2Kx2K UltraScan 894 CCD camera (Gatan) with a nominal magnification of 70000 and a pixel size of 2Å. The contrast transfer function (CTF) of each CCD image was determined using CTFFIND3 (Mindell and Grigorieff, 2003) and corrected by phase flip using CTFFINDA from the Image2000 package (Crowther et al., 1996). After manual particle selection, ~2300 selected particles were classified and averaged using the program "refine2d.py" in the EMAN suite (Ludtke et al., 1999). A 3D initial model was created using the program "startcsym" and further refined using "refine" from the EMAN suite (Ludtke et al., 1999).

For cryo-electron microscopy, either 2 μl of rATcpnβ (the purified rATcpnβ monomers were assembled into thermosomes with existence of ATP so this sample was placed in refrigerator for two weeks to make ATP fully hydrolyzed and released before plunge freezing) at 20 mg/ml or 3 μl of rATcpnβ·ATP·ALF_3 at 12 mg/ml was applied to a C-flat grid (r2/2, Protochips Inc., USA) and treated by the Solarus plasma cleaner system (Model 950, Gatan). The grids were then blotted and plunged into liquid ethane using a Vitrobot (FEI, Netherlands) running at 4°C and 95% humidity, transferred to a CT3500 cryo-holder (Gatan) and loaded into a Tecnai F20 FEG electron microscope (FEI, Netherlands). The electron microscope was operated at 120 kV and the rATcpnβ_apo and rATcpnβ_ATP samples were imaged using the LEGINON (Carragher et al., 2000; Suloway et al., 2005) automatic data acquisition system in the low dose mode. The images were recorded on a 4Kx4K UltraScan 895 CCD camera (Gatan) with a final pixel size of 1.55Å.

Tens of thousands of particles were automatically selected using FindEM (Roseman, 2004). The CTF of each micrographs was determined using CTFFIND3 (Mindell and Grigorieff, 2003) in the image2000 package (Crowther et al., 1996), and then the phases of each particle were corrected by using the “applyctf” program in the EMAN suite (Ludtke et al., 1999). After two-dimensional classification and averaging by the program "refine2d.py" in the EMAN suite, several bad classes with no clear structural information were discarded. The initial model was created using the program "startcsym" in EMAN. Three Gaussian noises under the same level were added into the initial model, resulting in three starting models, which were further refined by using “multirefine” in EMAN suite to remove the bad particles. Final refinements were performed using "refine" in EMAN with Spider scripts (Frank et al., 1996; Shaikh et al., 2008) embedded for correspondence analysis (CORAN) of each image class, wrapped in the Appion package (Lander et al., 2009). The final reconstructed density map was further sharpened by an amplitude correction algorithm using the program EM-BFACTOR (Fernandez et al., 2008). In summary, the rATcpnβ_apo reconstruction used ~46,000 particles in the final refinement, and for rATcpnβ_ATP, ~69,000 particles were used.

The resolutions of the above 3D reconstructions were assessed by the program RMEASURE (Sousa and Grigorieff, 2007) using the FSC 0.143 threshold. In addition, the suggested resolutions of the nsEM map of rATcpnβ, cryoEM map of rATcpnβ_apo and the cryoEM map of rATcpnβ_ATP are approximately 14Å, 8.8Å and 8.4Å respectively.

Crystallization of the rATcpnβ and post-crystal treatment

It should be mentioned that purified rATcpnβ monomers were assembled into thermosomes *in vitro* with existence of ATP so the sample used for crystallization contained ATP that was gradually hydrolyzed by rATcpnβ for one week. Purified rATcpnβ thermosome (6 mg/ml) was crystallized in 100 mM Tris-HCl, 1.2 M Li_2SO_4, at pH 8.0. Initially, leaf-shaped crystals were obtained with very weak diffraction. We optimized these rATcpnβ crystals by mixing 1 μl of protein solution (5 mg/ml rATcpnβ, 20 mM Tris-HCl pH 8.0, 5 mM EDTA-Na, 5 mM $MgCl_2$) and 1 μl of mother liquid (100 mM Tris-HCl, pH 8.5, 1.0 M Li_2SO_4) at 289 K over a 200-μl reservoir solution (100 mM Tris-HCl, pH 8.5, 1.15 M Li_2SO_4) by the

hanging drop vapor diffusion method. Some single crystals reached a size of 0.2 × 0.2 × 0.5 mm^3. The diffraction of the rATcpnβ crystals was dramatically improved by soaking them into a dehydration solution of 3.5 M ammonium sulfate for approximately 12 hr. Certain single, large crystals treated by dehydration could diffract to 6.0-4.5Å in-house, and then to 4.0~3.5Å in synchrotron radiation. After dehydration, the crystals were rapidly frozen in liquid nitrogen and stored for screening and data collection.

Data collection and processing

Diffraction data for the rATcpnβ crystal Form I were collected on a beamline BL-5A (detector Quantum 315 CCD) of the Photon Factory (Tsukuba, Japan) at a temperature of 100 K and using radiation of wavelength 1.000Å. Because of the large unit cell and the poorly diffracting, highly mosaic crystal, the data collection parameters were carefully selected and controlled. In particular, the crystal-to-detector distance was set to 530 mm and the oscillation angle was set to 0.3° for diffraction overlap minimization. The exposure time was optimized to 10 s to balance the diffraction resolution and radiation damage.

One year later, a diffraction data set for rATcpnβ crystal Form II was collected on the beam line BL-17A (detector Quantum 270 CCD) of the Photon Factory (Tsukuba, Japan) at a temperature of 100 K and using radiation of wavelength 0.900Å. The crystal-to-detector distance was set to 511.9 mm and the oscillation angle was set to 0.5°. The exposure time was optimized and set to 15 s.

The diffraction data sets were indexed, merged and scaled using the HKL2000 program suite (Otwinowski, 1997) for crystal Form I and MOSFLM (Powell, 1999) for Form II; the data processing statistics are summarized in Table 1.

Molecular replacement and structural refinement

Before diffraction data for crystal Form II were collected, the diffraction dataset of Form I was used to determine the crystal structure by molecular replacement. Fitting the complete coordinates of the subunits from the TAcpnα, TAcpnβ or TKcpn thermosomes into the cryoEM map of rATcpnβ did not yield a successful molecular replacement model. The correct starting model was manually built by fitting nine equatorial domains from the TKcpn subunits (pdb code: 1Q3R) into the cryoEM map of rATcpnβ_apo using UCSF Chimera (Goddard, 2007), which resulted in a single ring model. This model was used for molecular replacement with Phaser (A. J. McCoy, 2007), which produced several equivalent and significant solutions. The solution with the highest translational likelihood gain (6531), Z-score (36.4) and good crystal packing was selected for further phasing.

Initial phasing yielded a clear electron density around the equatorial domains, but a very poor and indiscriminate density around the other regions. The electron density map was dramatically improved by imposing the non-crystallographic symmetry (NCS) averaging technique, combined with phase extension from 10Å to 3.8Å and a small extension step of ~$0.002Å^{-1}$ in the reciprocal space. The averaged density map showed very good connectivity, and the secondary structures could be easily recognized. An initial poly-alanine model was built manually using Coot (Cowtan, 2004) under the guidance of the averaged map and topology of the TKcpn subunit. After rigid body refinement of the poly-alanine model by Refmac5 (Winn et al., 2001), another round of NCS averaging and phase extension was applied to produce further improved electron density, from which large residues such as Trp and Tyr could be distinguished. These residues were assigned and used as reference points in the sequence to locate other residues. Refinements (rigid body, simulated annealing, energy minimization and group B factor) of the manually built model were performed with CNS (A.T. Brunger, 1998; Brunger, 2007) using a NCS restriction

among the 27 subunits in one asymmetric unit. A negative B-factor (Brunger, 2006) ($-100Å^2$) was applied to sharpen the 2Fo-Fc map, which was further used to rebuild the model and correct some errors. The final structure of rTAcpnβ in crystal Form I was refined to 3.8Å with an Rwork of 36.5%, Rfree of 37.1% and an overall figure of merit (FOM) of 0.66.

The crystal structure of rTAcpnβ in Form II was solved by molecular replacement using the model from Form I. After several rounds of refinements, B-factor sharpening with a negative B-factor (Brunger, 2006) of $-70Å^2$ was applied to improve the electron density map, which was further used to correct some residues. The structure of rTAcpnβ in Form II was finally refined to 3.7Å with Rwork of 27.7%, Rfree of 28.3% and an overall figure of merit (FOM) of 0.78. The stereochemistry of the final model was checked using the program PROCHECK (Morris et al., 1992) with the result that 80.9% (369) of the residues are in most favored regions, 17.8% (81) are in allowed regions and 1.3% (6) are in generously allowed regions. The statistics for the structural refinements are summarized in Table 1.

Protease K digestion assay

The assay buffer was 50mM Tris-HCl, pH7.4, 100 mM KCl and 25 mM $MgCl_2$. Chaperonins (0.35mg/ml) were incubated without or with ADP (1mM), ATP (1mM), ADP (1mM) / NaF (30mM) / $AlCl_3$ (5mM), ATP (1mM) /) / NaF (30mM) / $AlCl_3$ (5mM), respectively, for 20 min at 75°C. Then digestion with protease K (20 ng/μl) was performed at 65°C for 5 min. Then PMSF (phenylmethylsulfonyl fluoride) was added into the mixture with final concentration 5mM to inhibit the digestion of protease K before the sample was analyzed on 12.5% SDS-PAGE. Gels were stained with Coomassie Brilliant Blue.

Structural analysis and illustration

All structural superposition calculations were performed using the “align” command in PyMol(DeLano, 2002). The solvent accessible surface areas and interface areas of the thermosome subunits were calculated by the program PISA(Krissinel and Henrick, 2007). The EM maps were segmented, displayed and fitted with crystal structures using UCSF Chimera(Pettersen et al., 2004).

All structural figures were generated by UCSF Chimera(Pettersen et al., 2004), Molscript (P. J. Kraulis, 1991), Bobscript (Esnouf, 1997)and PyMol(DeLano, 2002) indicated.

Supplementary Material

Refer to Web version on PubMed Central for supplementary material.

Acknowledgments

We would like to thank Dr. Lingpeng Cheng (Institute of Biophysics, Chinese Academy of Sciences) for his help with UCSF Chimera and Ruigang Su (F.S. group) for his help preparing carbon-coated grids. This work was supported by NSFC grant (30770496, 30721003), “973” project (2006CB806506, 2006CB911001), Chinese Academy of Sciences (KGCX1-YW-13) and "863" project (2007AA100604). The author gratefully acknowledges the support of K. C. Wong Education Foundation, Hong Kong (to Fei Sun). CryoEM datasets were collected at the National Resource for Automated Molecular Microscopy, which is supported by the National Institute of Health through the National Center for Research Resources’ P41 program (RR17573).

ABBREVIATIONS

cryoEM	cryo-electron microscopy
nsEM	Negative staining electron microscopy

rATcpnβ	recombinant thermosome from *Acidianus tengchongensis*
TAcpn	thermosomes from *T.acidophilum*
TKcpn	thermosomes *thermococcus sp.* strain KS-1
CCT	chaperonin containing TCP-1
TB	Terrific Broth medium
IPTG	Isopropyl β-D-1-thiogalactopyranoside
PAGE	polyacrylamide gel electrophoresis

REFERENCES

McCoy AJ, RW G-K, Adams PD, Winn MD, Storoni LC, Read RJ. Phaser crystallographic software. J. Appl. Cryst 2007;40:658–674. [PubMed: 19461840]

Brunger AT, A PD, Clore GM, Gros P, Grosse-Kunstleve RW, Jiang J-S, Kuszewski J, Nilges N, Pannu NS, Read RJ, Rice LM, Simonson T, Warren GL. Crystallography & NMR System (CNS), A new software suite for macromolecular structure determination. Acta Crystallographica 1998;D54:905–921.

Bigotti MG, Clarke AR. Chaperonins: The hunt for the Group II mechanism. Archives of biochemistry and biophysics 2008;474:331–339. [PubMed: 18395510]

Booth CR, Meyer AS, Cong Y, Topf M, Sali A, Ludtke SJ, Chiu W, Frydman J. Mechanism of lid closure in the eukaryotic chaperonin TRiC/CCT. Nature structural & molecular biology 2008;15:746–753.

Brunger AT. Version 1.2 of the Crystallography and NMR System. Nature Protocols 2007;2:2728–2733.

Brunger, BDaAT. Considerations for the refinement of low-resolution crystal structures. Acta Crystallographica 2006;D62:923–932.

Bukau B, Horwich AL. The Hsp70 and Hsp60 chaperone machines. Cell 1998;92:351–366. [PubMed: 9476895]

Carragher B, Kisseberth N, Kriegman D, Milligan RA, Potter CS, Pulokas J, Reilein A. Leginon: an automated system for acquisition of images from vitreous ice specimens. J Struct Biol 2000;132:33–45. [PubMed: 11121305]

Clare DK, Stagg S, Quispe J, Farr GW, Horwich AL, Saibil HR. Multiple states of a nucleotide-bound group 2 chaperonin. Structure 2008;16:528–534. [PubMed: 18400175]

Cowtan, PEaK. Coot: model-building tools for molecular graphics. Acta Cryst 2004;60:2126–2132.

Crowther RA, Henderson R, Smith JM. MRC image processing programs. J Struct Biol 1996;116:9–16. [PubMed: 8742717]

DeLano, WL. PyMOL Molecular Viewer. 2002. http://www.pymol.org

Ditzel L, Lowe J, Stock D, Stetter KO, Huber H, Huber R, Steinbacher S. Crystal structure of the thermosome, the archaeal chaperonin and homolog of CCT. Cell 1998;93:125–138. [PubMed: 9546398]

Esnouf RM. An extensively modified version of MolScript that includes greatly enhanced coloring capabilities. Journal of molecular graphics & modelling 1997;15:132–134. 112–133. [PubMed: 9385560]

Fernandez JJ, Luque D, Caston JR, Carrascosa JL. Sharpening high resolution information in single particle electron cryomicroscopy. Journal of structural biology 2008;164:170–175. [PubMed: 18614378]

Frank J, Radermacher M, Penczek P, Zhu J, Li Y, Ladjadj M, Leith A. SPIDER and WEB: processing and visualization of images in 3D electron microscopy and related fields. Journal of structural biology 1996;116:190–199. [PubMed: 8742743]

Frydman J, Nimmesgern E, Erdjument-Bromage H, Wall JS, Tempst P, Hartl FU. Function in protein folding of TRiC, a cytosolic ring complex containing TCP-1 and structurally related subunits. The EMBO journal 1992;11:4767–4778. [PubMed: 1361170]

Gao Y, Thomas JO, Chow RL, Lee GH, Cowan NJ. A cytoplasmic chaperonin that catalyzes beta-actin folding. Cell 1992;69:1043–1050. [PubMed: 1351421]

Goddard TD. Visualizing density maps with UCSF Chimera. Journal of Structural Biology 2007;157:281–287. [PubMed: 16963278]

Hemmingsen SM, Woolford C, van der Vies SM, Tilly K, Dennis DT, Georgopoulos CP, Hendrix RW, Ellis RJ. Homologous plant and bacterial proteins chaperone oligomeric protein assembly. Nature 1988;333:330–334. [PubMed: 2897629]

Iizuka R, Yoshida T, Shomura Y, Miki K, Maruyama T, Odaka M, Yohda M. ATP binding is critical for the conformational change from an open to closed state in archaeal group II chaperonin. The Journal of biological chemistry 2003;278:44959–44965. [PubMed: 12920124]

Kim S, Willison KR, Horwich AL. Cystosolic chaperonin subunits have a conserved ATPase domain but diverged polypeptide-binding domains. Trends in biochemical sciences 1994;19:543–548. [PubMed: 7846767]

Klumpp M, Baumeister W, Essen LO. Structure of the substrate binding domain of the thermosome, an archaeal group II chaperonin. Cell 1997;91:263–270. [PubMed: 9346243]

Krissinel E, Henrick K. Inference of macromolecular assemblies from crystalline state. Journal of molecular biology 2007;372:774–797. [PubMed: 17681537]

Lander GC, Stagg SM, Voss NR, Cheng A, Fellmann D, Pulokas J, Yoshioka C, Irving C, Mulder A, Lau PW, et al. Appion: an integrated, database-driven pipeline to facilitate EM image processing. Journal of structural biology 2009;166:95–102. [PubMed: 19263523]

Lauerer G, Kristjansson JK, Langworthy TA, Stetter KO. Methanothermus sociabilis sp. Nov., a second species within the methanothermaceae growing at 97 °C. Systematic and applied microbiology 1986;8:100–105.

Llorca O, Smyth MG, Carrascosa JL, Willison KR, Radermacher M, Steinbacher S, Valpuesta JM. 3D reconstruction of the ATP-bound form of CCT reveals the asymmetric folding conformation of a type II chaperonin. Nature structural biology 1999;6:639–642.

Ludtke SJ, Baldwin PR, Chiu W. EMAN: semiautomated software for high-resolution single-particle reconstructions. J Struct Biol 1999;128:82–97. [PubMed: 10600563]

Mindell JA, Grigorieff N. Accurate determination of local defocus and specimen tilt in electron microscopy. J Struct Biol 2003;142:334–347. [PubMed: 12781660]

Morris AL, MacArthur MW, Hutchinson EG, Thornton JM. Stereochemical quality of protein structure coordinates. Proteins 1992;12:345–364. [PubMed: 1579569]

Nitsch M, Walz J, Typke D, Klumpp M, Essen LO, Baumeister W. Group II chaperonin in an open conformation examined by electron tomography. Nature structural biology 1998;5:855–857.

Ochman H, Gerber AS, Hartl DL. Genetic applications of an inverse polymerase chain reaction. Genetics 1988;120:621–623. [PubMed: 2852134]

Otwinowski ZMW. Processing of X-ray diffraction data collected in oscillation mode. Methods Enzymol 1997:276.

Kraulis PJ. MOLSCRIPT: a program to produce both detailed and schematic plots of protein structures. J. Appl. Cryst 1991;24:946–950.

Pettersen EF, Goddard TD, Huang CC, Couch GS, Greenblatt DM, Meng EC, Ferrin TE. UCSF Chimera--a visualization system for exploratory research and analysis. Journal of computational chemistry 2004;25:1605–1612. [PubMed: 15264254]

Phipps BM, Hoffmann A, Stetter KO, Baumeister W. A novel ATPase complex selectively accumulated upon heat shock is a major cellular component of thermophilic archaebacteria. The EMBO journal 1991;10:1711–1722. [PubMed: 1828761]

Powell HR. The Rossmann Fourier autoindexing algorithm in MOSFLM. Acta Crystallogr D Biol Crystallogr 1999;55:1690–1695. [PubMed: 10531518]

Ranson NA, Clare DK, Farr GW, Houldershaw D, Horwich AL, Saibil HR. Allosteric signaling of ATP hydrolysis in GroEL-GroES complexes. Nature structural & molecular biology 2006;13:147–152.

Roseman AM. FindEM--a fast, efficient program for automatic selection of particles from electron micrographs. J Struct Biol 2004;145:91–99. [PubMed: 15065677]

Schoehn G, Quaite-Randall E, Jimenez JL, Joachimiak A, Saibil HR. Three conformations of an archaeal chaperonin, TF55 from Sulfolobus shibatae. Journal of molecular biology 2000;296:813–819. [PubMed: 10677283]

Shaikh TR, Gao H, Baxter WT, Asturias FJ, Boisset N, Leith A, Frank J. SPIDER image processing for single-particle reconstruction of biological macromolecules from electron micrographs. Nature protocols 2008;3:1941–1974.

Shomura Y, Yoshida T, Iizuka R, Maruyama T, Yohda M, Miki K. Crystal structures of the group II chaperonin from Thermococcus strain KS-1: steric hindrance by the substituted amino acid, and inter-subunit rearrangement between two crystal forms. Journal of molecular biology 2004;335:1265–1278. [PubMed: 14729342]

Sousa D, Grigorieff N. Ab initio resolution measurement for single particle structures. J Struct Biol 2007;157:201–210. [PubMed: 17029845]

Suloway C, Pulokas J, Fellmann D, Cheng A, Guerra F, Quispe J, Stagg S, Potter CS, Carragher B. Automated molecular microscopy: the new Leginon system. J Struct Biol 2005;151:41–60. [PubMed: 15890530]

Tilly K, Murialdo H, Georgopoulos C. Identification of a second Escherichia coli groE gene whose product is necessary for bacteriophage morphogenesis. Proceedings of the National Academy of Sciences of the United States of America 1981;78:1629–1633. [PubMed: 7015340]

Wang L, Hu ZJ, Luo YM, Huo YW, Ma Q, He YZ, Zhang YY, Sun F, Dong ZY. Distinct symmetry and limited peptide refolding activity of the thermosomes from the acidothermophilic archaea Acidianus tengchongensis S5(T). BBRC 2010;393:228–234. [PubMed: 20117082]

Winn MD, Isupov MN, Murshudov GN. Use of TLS parameters to model anisotropic displacements in macromolecular refinement. Acta Crystallogr D Biol Crystallogr 2001;57:122–133. [PubMed: 11134934]

Wittig I, Braun HP, Schagger H. Blue native PAGE. Nat Protoc 2006;1:418–428. [PubMed: 17406264]

Xu Z, Horwich AL, Sigler PB. The crystal structure of the asymmetric GroEL-GroES-(ADP)7 chaperonin complex. Nature 1997;388:741–750. [PubMed: 9285585]

Yaffe MB, Farr GW, Miklos D, Horwich AL, Sternlicht ML, Sternlicht H. TCP1 complex is a molecular chaperone in tubulin biogenesis. Nature 1992;358:245–248. [PubMed: 1630491]

Zhang J, Baker ML, Schroder GF, Douglas NR, Reissmann S, Jakana J, Dougherty M, Fu CJ, Levitt M, Ludtke SJ, et al. Mechanism of folding chamber closure in a group II chaperonin. Nature 2010;463:379–383. [PubMed: 20090755]

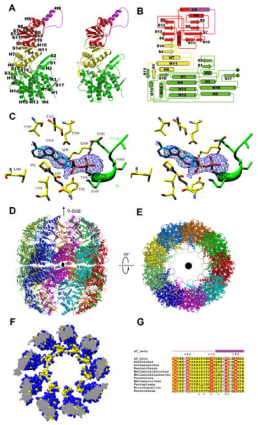

Figure 1.

Crystal structure of rATcpnβ. (A) Structural features of the rATcpnβ monomer, colored by domain. The lid is purple, apical domain is red, intermediate domain is yellow and the equatorial domain is green. The modeled ADP is colored by element. (B) Topology of rATcpnβ monomer. (C) The stereo view of nucleotide binding site of rATcpnβ. The 2Fo-Fc omit difference map (contour level 0.8) shows an elongated stretch of electron density on top of the equatorial domain, into which the ADP could be modeled. The adjacent residues involved in interaction are labeled. (D, E) Side and top views of overall rATcpnβ structure. (F) Hydrophobic patch in the lid domain of group II chaperonin. Hydrophobic surface representation of rATcpnβ crystal structure. The hydrophobic surface is colored by yellow and the hydrophilic by blue. (G) Sequence alignments of thermosomes across several species reveal hydrophobic patch in the lid is conserved and corresponding site is indicated in green triangle. The genbank accessions of protein sequences form top to bottom are AAO47380, YP_255343, YP_003400009, NP_963436, YP_003459021, NP_275933, NP_142040, YP_001048251, ZP_05570324, ABX13688 and ACB08055 respectively. See also Figure S1.

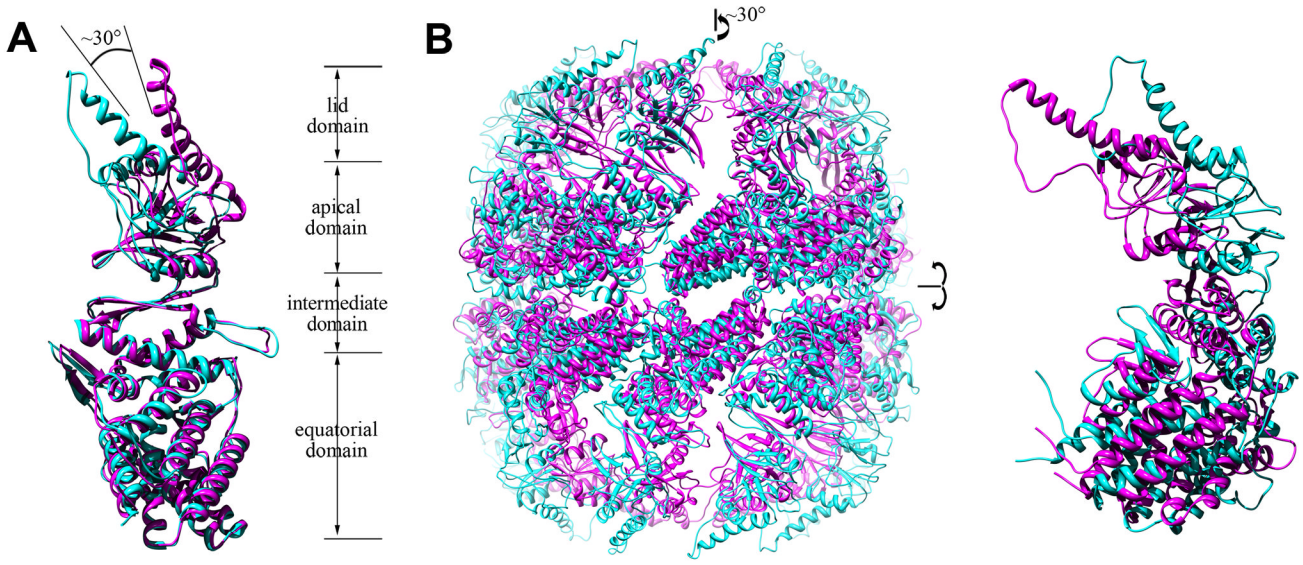

Figure 2.

Comparison of the monomer and overall structures of the two thermosome states. (A) The rATcpnβ crystal structure is an open state colored in cyan. The TKcpn crystal structure represents the closed state colored in pink. (B) Superposition of the overall structures for rATcpnβ in the open state (cyan) and closed state (pink) based on the cryoEM and nsEM map, respectively. One isolated subunit is enlarged and shown on the right. See also Figure S2 and Movie S1 to S5.

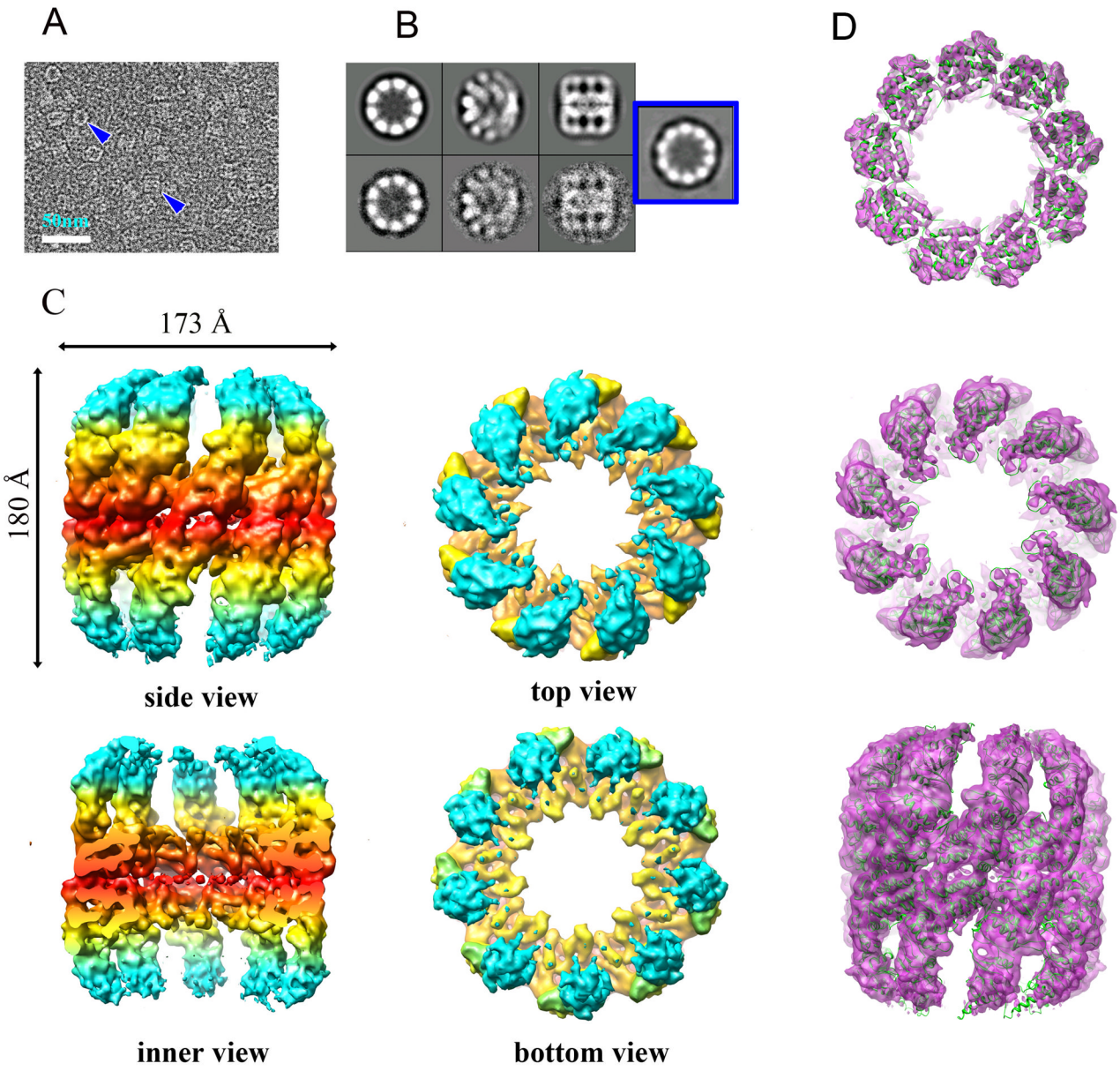

Figure 3.

CryoEM structure of rATcpnβ in open state and atomic structure fitting. (A) Raw image of particles in cryo-EM. Top and side views are indicated by blue arrows. The scale bar is 50nm. (B) Averaging views (top, tilt and side) of selected 2D classes of cryoEM particles of rATcpnβ_ATP are matched to the corresponding 3D projections. The top view exhibiting 10-fold symmetry, with a small portion (~10%) from 2D classification indicated in the blue square. (C) Surface representation of the side, inner, top and bottom views of the cryo-EM structure of rATcpnβ_ATP. The cryo-EM structure of rATcpnβ_apo is similar to rATcpnβ_ATP and not shown here. EM map are colored based on domain division, with the apical and lid domains in cyan, the intermediate domain in yellow, and the equatorial domain in red. (D) equatorial, apical domain and side views of the rATcpnβ subunit crystal structure fit into the rATcpnβ_ATP cryoEM map. See also Figure S3 to S5.

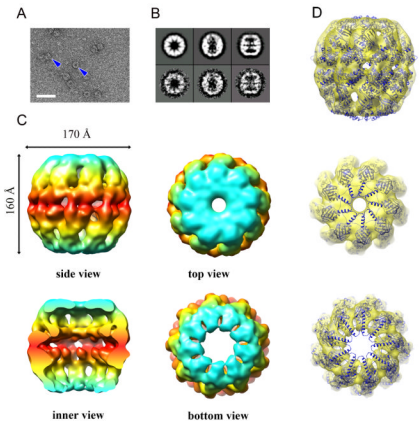

Figure 4.

Negative staining EM structure of rATcpnβ in closed state and atomic structure fitting. (A) Raw EM image of negatively stained particles. Top and side views are indicated by blue arrows. The scale bar is 50nm. (B) Averaging views (top, tilt and side) of selected 2D classes of the negatively stained particles are matched to the corresponded 3D projections. (C) Surface representation of the side, inner, top, and bottom views of the negative stain structure. EM map are colored based on domain division, with the apical and lid domains in cyan, the intermediate domain in yellow, and the equatorial domain in red. (D) Side, top, and bottom views of the TKcpn subunit crystal structure fit into the rATcpnβ nsEM map. See also Figure S4 to S5.

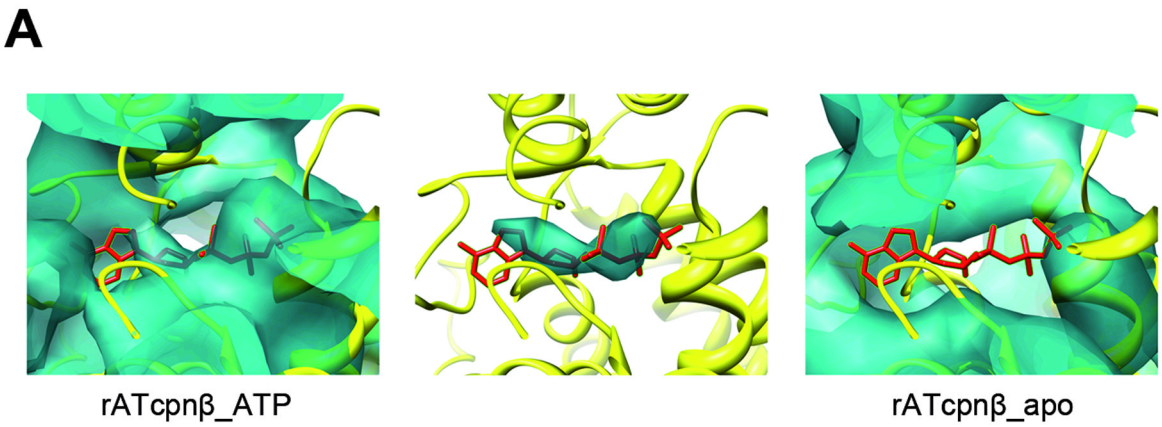

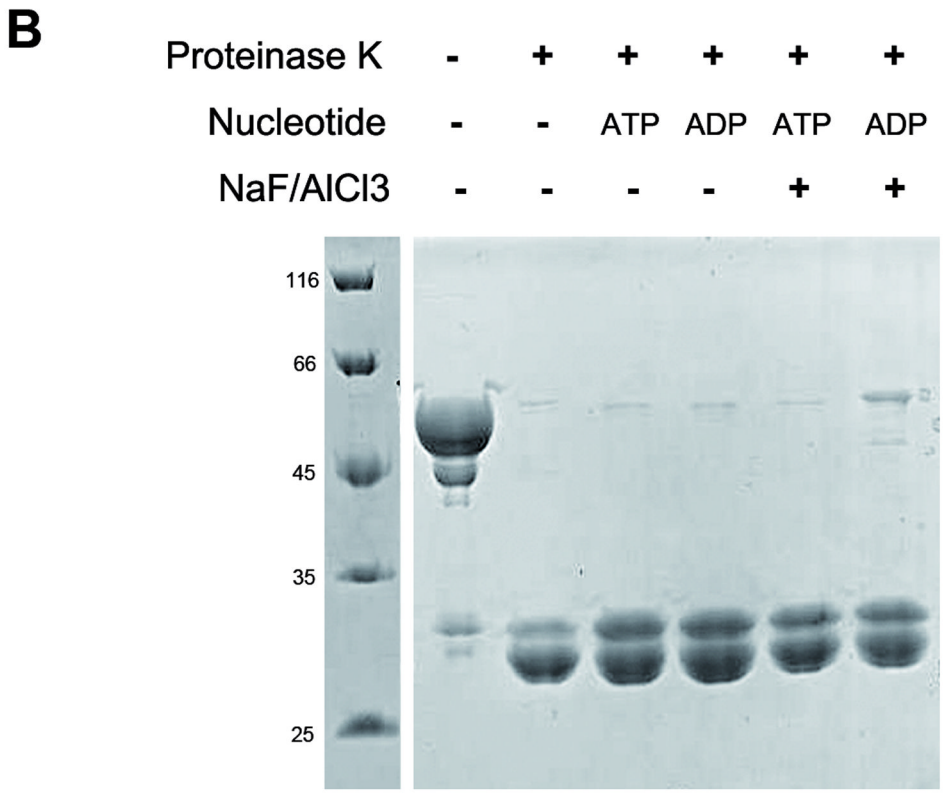

Figure 5.

ATP binding without hydrolysis could not trigger a closed structure for group II chaperonin. (A) A comparison of the electron density near the ATP binding sites of the rATcpnβ_apo and rATcpnβ_ATP cryoEM maps. On the left the rATcpnβ crystal structure is fitted into the rATcpnβ_ATP cryoEM map. The middle shows the difference map between the rATcpnβ_ATP cryoEM map and the rATcpnβ crystal structure with ADP omitted. The right shows the rATcpnβ crystal structure is fitted into the rATcpnβ_apo cryoEM map. ATP shown as red stick model is placed into the nucleotide binding pocket. (B) Protease K digestion assay of rATcpnβ under different conditions. The rATcpnβ incubated with ADP,

ATP, ADP/NaF/$AlCl_3$ or ATP/NaF/$AlCl_3$ were digested by protease K at 65°C for 5min.Each lane is labeled and self-explanatory.

Table 1

Table X-ray diffraction data collection and refinement statistics [a]

Data collection	**Form I**	**Form II**
Space group	C2	C2
Cell dimensions		
a, b, c (Å)	501.0, 276.3, 161.0	223.7, 283.0, 160.8
alpha,beta,gamma (°)	90.00, 106.8, 90.00	90.0, 133.9, 90.0
Resolution (Å)	50.0-3.80 (3.94-3.80)	50.0-3.70 (3.90-3.70)
R_{merge} [b]	0.181 (0.390)	0.117 (0.476)
I/σ	9.0 (1.6)	7.4 (2.3)
Completeness (%)	97.0 (81.4)	99.5(99.4)
Redundancy	3.2 (2.5)	3.2 (3.3)
Refinement		
Resolution (Å)	50.0-3.80	50.0-3.70
No. reflections	199,545	76576
R_{work}/R_{free} (%) [c]	36.5/37.1	27.7/28.3
No. atoms		
Protein (one subunit)	3849	3849
Ligand/ion (ADP)	—	27
B-factors (Å^2)		
Equator domain	70.4	108.5
Median domain	108.1	135.0
Apical domain	112.0	137.2
Lid domain	118.8	147.1
r.m.s. deviations		
Bond lengths (Å)	0.01	0.01
Bond angles (°)	1.41	1.48

[a] Corresponding parameters for the highest-resolution shell are shown in parentheses.

[b] $R_{merge} = \Sigma_h \Sigma_i |I_{ih} - \langle I_h \rangle| / \Sigma_h \Sigma_i \langle I_h \rangle$, where $\langle I_h \rangle$ is the mean intensity of the observation I_{ih} reflection h.

[c] $R_{work} = \Sigma(||\mathbf{F}_p(obs)| - |\mathbf{F}_p(calc)||) / \Sigma|\mathbf{F}_p(obs)|$; R_{free} = R factor for a selected subset (5%) of the reflections that was not included in prior refinement calculations.